

# Seismic reservoir characterization of Duvernay shale with quantitative interpretation and induced seismicity considerations – a case study

Satinder Chopra<sup>\*†</sup>, Ritesh Kumar Sharma<sup>†</sup>, Amit Kumar Ray<sup>#</sup>, Mohammad Nemati<sup>†</sup>, Ray Morin<sup>+</sup>, Brian Schulte<sup>+</sup> and David D'Amico<sup>+</sup>

<sup>†</sup>Arcis Seismic Solutions, TGS, Calgary; <sup>+</sup>Repsol Oil and Gas Canada, Calgary; <sup>#</sup>formerly at Arcis Seismic Solutions, TGS, Calgary

## Summary

The Devonian Duvernay Formation in northwest central Alberta, Canada has become a hot play in the last few years due to its richness in both liquid and gaseous hydrocarbon resources. The oil and gas generation in this shale formation made it the source rock for many oil and gas fields in its vicinity. This case study attempts to showcase the characterization of Duvernay Formation by using 3D multicomponent seismic data, and integrating it with the available well log and other relevant data. This characterization has been done by deriving rock physics parameters (Young's modulus, Poisson's ratio, etc.) through deterministic simultaneous and joint impedance inversion, with appropriate quantitative interpretation. In particular, we determine the brittleness of the Duvernay interval which helps us determine the sweet spots therein. The scope of this characterization exercise was extended to explore the induced seismicity observed in the area (i.e. earthquakes of magnitude >3), that is perceived to be associated with hydraulic fracture stimulation of the Duvernay. This has been a cause of media coverage lately. We attempt to integrate our results with the induced seismicity data available in the public domain, and have obtained reasonably convincing results.

## Introduction

The Duvernay shale in Alberta, Canada has been the source rock for many of the larger Devonian oil and gas fields in Alberta, including the oil and gas producing Leduc and Nisku formations. The area of focus in this study is located in the Kaybob and Fox Creek areas of west central Alberta, which is about 250 km northwest of Edmonton (Figure 1). In and around the Kaybob area, the Duvernay shale lying at a depth of 3000-3500 m, is sufficiently mature and charged with liquids-rich gas to make it economically attractive. Besides thermal maturity, there are other favourable key elements such as richness, thickness and type of organic material in the rock, the reservoir quality, the depth and pressure, which, when combined, define the so-called sweet spots in the Duvernay liquids-rich formation. The main goal for shale resource characterization is usually the identification of these sweet spots which represent the most favourable drilling targets. For the present study the available 3D-3C seismic data was acquired in early 2015. After processing, it was made available for reservoir characterization and quantitative interpretation late last year. This seeks to quantify the reservoirs by understanding elastic properties, lithology, fluid content and geometrical distribution. Such quantification can be carried out by way of P- and S-impedance determination, combined with petrophysical parameters available at the location of the wells. Good well control is critical, but in some cases is not available. Attempts at quantitative interpretation of seismic data can result in considerable value addition to which is the goal of this case study. A workflow for performing quantitative seismic interpretation

(Chopra, 2015) for the Duvernay shale was chalked out, and care was taken to carry out more detailed analysis at each step.

## Well log correlation

The Duvernay shale is a fine-grained and silica-rich shale unit which is overlaid by the Ireton (calcareous) and Winterburn shale units, and over which lies the Wabamun limestone unit. The Duvernay unit is underlain by a thin carbonate-rich shale layer that overlies the Swan Hills reefal unit. The stratigraphic column shown to the left of Figure 2 illustrates these units. In the same figure we see the correlation of P-velocity, density, and Gamma Ray curves (Figure 2a), and the synthetic seismogram (Figure 2b) with stacked seismic data (Figure 2c). We notice a good correlation overall.

## Preconditioning of seismic data

The seismic data (both PP and PS) were conditioned carefully to make sure that amplitudes are preserved such that their variation with offset/angle could be utilized in a meaningful way. The different processes employed in the conditioning were supergathering (3x3), bandpass filtering, random noise attenuation and trim statics, with difference plots taken at each step to ensure that no leakage of useful signal goes through. In Figure 3 we show a modeled PP elastic gather being compared with the real seismic gather before and after conditioning. Notice the enhancement in the signal-to-noise ratio after conditioning. Similar conditioning was undertaken for the PS seismic gathers.

## Low-frequency trend determination for impedance inversion

While carrying out impedance inversion, the addition of a low-frequency trend is necessary for obtaining absolute values of impedance. The usual practice is to low-pass filter (< 10 Hz) the available impedance well log curves and use one or more of the derived curves for generation of the low-frequency trend volume using extrapolation or interpolation and guided by horizon boundaries. When more than one well is used for the generation of the low-frequency trend, the commonly used methods (e.g. inverse-distance weighted schemes) could produce artifacts. We instead make use of a relatively new approach (Ray et al., 2015) for this low-frequency trend generation which makes use of both well log data and seismic data to establish a relationship between seismic attributes and the available well log curves. Figure 4a shows a comparison of the predicted or generated low-frequency impedance trend using multiregression analysis with the filtered low frequency impedance curve for blind well W-3. The two seem to match reasonably well. In Figure 4b, we show the horizon slice display at the Duvernay level, from the lower frequency impedance volume. Notice the gradual change between the northwest and southeast quadrants, perhaps suggesting increased interference from the Swan Hills trend that exists below this level.

*Simultaneous inversion*

In simultaneous prestack inversion, multiple partial-offset or angle substacks are inverted simultaneously. For each angle stack, a unique wavelet is estimated. Subsurface low-frequency models for P-impedance, S-impedance and density, constrained with appropriate horizons in the broad zone of interest, are constructed using the approach explained above. The models, wavelets and partial stacks were used as input in the inversion, and the output are P-impedance, S-impedance and density.

*Joint inversion*

Inversion of P-wave data together with S-wave data is referred to as *joint inversion*. Joint inversion makes use of the amplitudes and travel times of the P-wave and S-wave data for estimating P-impedance, S-impedance and density to provide a more robust inversion result.

After processing of multicomponent seismic data, the outputs are PP wave data processed in PP two-way time and PS wave data processed in PS time scale. For continuing any consistent analysis, the next step is to perform an accurate PP and PS time correspondence, a process referred to as *registration*. It is usually done by matching the corresponding correlative events on the PP and PS data volumes, and then mapping or shrinking the PS time scale to the PP time scale. In Figure 5 we show the well-to-seismic correlation for PS data at well W-3. The well log curves are shown in Figure 5a, and the PS synthetic seismogram (blue traces) correlation with real PS seismic data (red traces) is seen in Figure 5b. The correlation between the two was found to be 93%, which is very encouraging. A segment of the PS data in PS time is shown in Figure 5c.

Once the well-to-seismic correlation for both PP and PS data is done satisfactorily, the depth-time curves for both are determined. The  $\frac{V_p}{V_s}$  ratio determined this way is valid at the location of the well only. Using this information, the PP data with its horizons (in blue) are stretched to PS time, and displayed alongside PS data (in PS time) as in Figure 5d. This helps identifying the corresponding horizons on the PS data, and the trackable horizons are then picked as is shown in magenta colour (Figure 5c). The horizons picked on PP and PS data will match at the location of the wells, but laterally may exhibit travel-time differences. Such differences are determined for the various intervals bounded by horizons and  $V_p/V_s$  ratios are determined for those intervals.

The  $V_p/V_s$  volume generated at the Duvernay level via the PP-PS registration was confirmed at a few blind wells and so was taken to be accurate. Joint inversion can be carried out with poststack as well as prestack multicomponent seismic data. For poststack joint inversion the inputs are the PP stacked data, the PS stacked data, the wavelets extracted from the two datasets in the broad zone of interest, and the P-impedance and S-impedance models. While the PP stack is the normal incidence data, PS data may be taken as the stack at say 12° or 15°, where the mode conversion sets in. The reflectivities modeled at 0° and 15° and convolved with the appropriate wavelets are compared with the real PP and PS seismic data and the error between them is minimized in a least squares sense. In the case of prestack joint inversion, usually three or five angle-limited stacks are first generated. Modeled reflectivities at

these angles are generated, compared with the real data and the error is then iteratively minimized in a least squares sense. In each case the output from joint inversion was P-impedance, S-impedance and density data (Chopra and Sharma, 2015). Equivalent segments of P-impedance sections passing through well W-3 from simultaneous, poststack joint and prestack joint inversion are shown in Figure 6. The impedance log curve filtered to seismic bandwidth is overlaid on the individual sections, both in the form of a curve as well as a coloured strip. The correlation between the well impedance and the inverted impedance looks good.

**Impedance inversion analysis**

The P- and S-impedance volumes obtained from the different types of inversion were again subjected to QC checks at the blind well locations and then put through rock physics analysis on the derived attributes. A common QC is to crossplot the log-derived P- and S-impedance values at the different wells against the seismic-derived impedance values at those locations. A correlation coefficient comparison for different inversion methods is exhibited in Table 1. Notice that the correlation coefficients increase as we go from simultaneous inversion to prestack joint inversion, which is what is expected from multicomponent seismic data in terms of value-addition.

**Table 1:** Comparison of correlation coefficients evaluated from crossplots for P- and S-impedance from well log data and inverted seismic data.

Well W-1	Simultaneous inversion	Post-stack joint inversion	Pre-stack joint inversion
P-impedance	0.952420	0.931485	0.968957
S-impedance	0.945133	0.960941	0.977858

**Brittleness determination for the Duvernay**

Amongst the different physical parameters that characterize the rocks, the two important ones for brittleness determination are Young’s modulus ( $E$ ) and Poisson’s ratio ( $\nu$ ).

Grieser and Bray (2007) showed that brittleness average can be computed from Young’s modulus and Poisson’s ratio as  $\left(\frac{E_B + \nu_B}{2}\right)$ , where

$$E_B = \frac{(E - E_{min})}{2(E_{max} - E_{min})}, \text{ and } \nu_B = \frac{(\nu - \nu_{max})}{2(\nu_{min} - \nu_{max})}.$$

Following this approach we computed the brittleness average volume and then generated a strata slice at the Duvernay level by averaging the attribute over a small time interval (10 ms) as shown in Figure 7a. Pockets with high values of brittleness are indicated in purple colour.

**Induced seismicity in the Fox Creek area**

The Fox Creek area in Alberta has been in the news recently due to earthquakes of magnitude above 4. Recent studies demonstrate that cases of induced seismicity are highly correlated with hydraulic fracturing (HF) (Atkinson et al., 2016) and the common perception is that in the Fox Creek area they are triggered by HF of the Duvernay formation. Injection of fluid, whether by HF or waste water disposal will result in higher interstitial pressure or pore pressure which, beyond the cracking of rock may result in reactivating already existing fractures or faults. All these

observations are suggestive that the seismic data should be extensively examined for the indications of faults and fractures. An initial straightforward approach is to determine discontinuities in the 3D seismic data volume by way of coherence, curvature, and brittleness (or other) attribute volumes. This was performed but the initial strat-cube analysis at the Duvernay level showed no visible indication of any faults or fractures on the coherence display. The curvature displays do indicate a number of lineaments, which can be further studied for any possible connection with fault reactivation. At the present time, such a detailed conclusive study has not been carried out.

To take this analysis forward, we overlaid some seismicity data available from the AER website, on the brittleness and curvature displays as shown in Figure 7. Interestingly, the seismicity patterns do seem to fall more often on the high brittleness pockets. However, there seems to be no strong correlation of the events with the curvature. While the displays in Figure 7 may show promise, we point out that the exact depth from where each earthquake originated cannot be ascertained. What this implies is that the display we are showing in Figure 7, may be suspect, and the data need to be further examined carefully.

**Conclusions**

We have carried out seismic reservoir characterization of the Duvernay shale formation in the Fox Creek area of Alberta, using multicomponent seismic data. The seismic attributes derived therefrom have enabled us to integrate the available induced seismicity data from the public domain, and attempt to draw some valid conclusions. The resulting brittleness attribute seems convincing, though questions about the depth accuracy of the induced seismicity data do remain. We make the case that surface seismic data together with its integration with other relevant data can help characterize the Duvernay shale formation.

**Acknowledgements**

We thanks Arcis Seismic Solutions, TGS, Calgary, for permission to present this work.

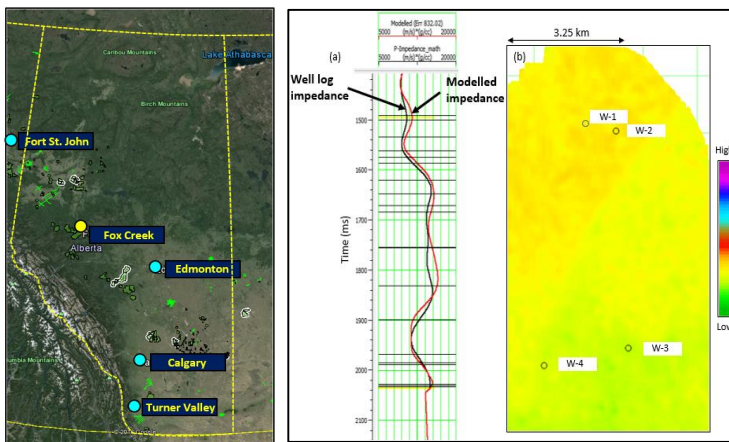


Figure 1: Location of 3D seismic data in Fox Creek study area, Alberta, Canada. (Image generated using Google Earth)

Figure 4: (a) Prediction of low frequency P-impedance trend for blind well W-3 using multi-attributes regression analysis and its comparison with the real P-impedance well log curve; (b) Horizon slice from the low-frequency trend volume at the Duvernay level. Notice the gradual variation of P-impedance seen on the slice. (Data courtesy: Arcis Seismic Solutions, TGS, Calgary)

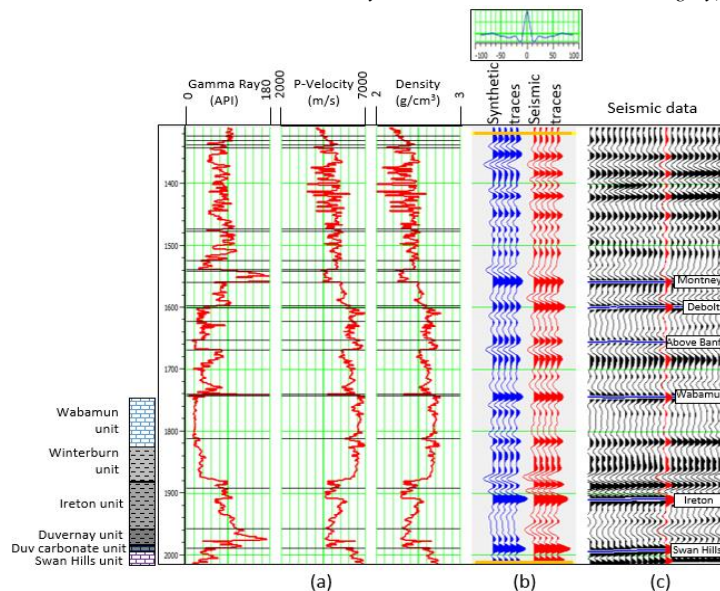


Figure 2: Correlation of W-2 well log curves with seismic data. Blue traces represent the synthetics (generated with the wavelet shown above) while the red traces represent the seismic data. The correlation coefficient between the synthetic and red traces in the time window indicated by the yellow bars is 0.82, suggesting an overall good correlation. (Data courtesy: Arcis Seismic Solutions, TGS, Calgary)

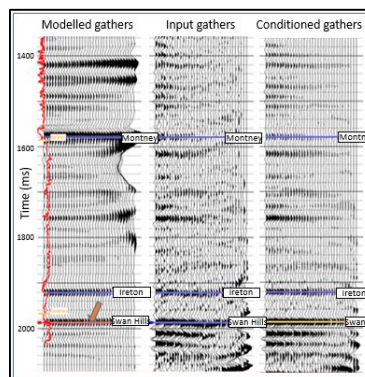


Figure 3: Comparison between modelled gathers at the location of well W-3, and the equivalent input gathers, and conditioned gathers. (Data courtesy: Arcis Seismic Solutions, TGS, Calgary)

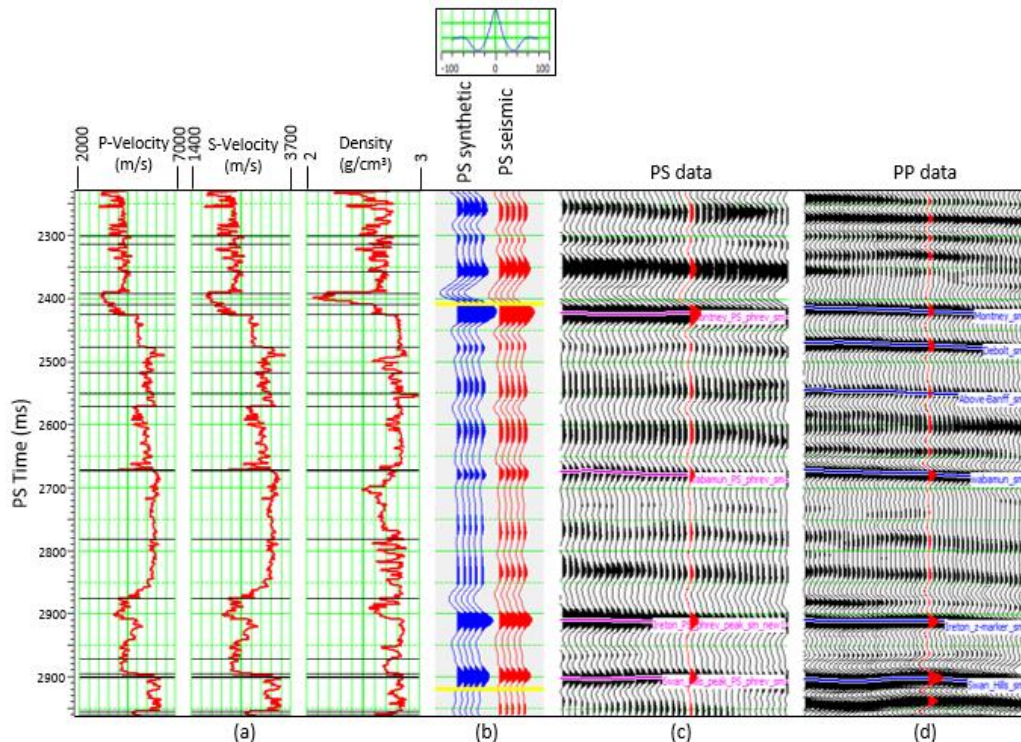


Figure 5: Well-to-seismic correlation for PS data as well as registration with PP data, at well W-3. The PS synthetic seismogram (blue traces) is shown in Figure 5b correlated with PS real seismic traces (in red). The displayed wavelet, used for generation of the synthetic seismogram, was extracted from the PS seismic data using a statistical process. The PS (Figure 5c) and PP (Figure 5d) data are shown both in PS time. (Data courtesy: Arcis Seismic Solutions, TGS, Calgary)

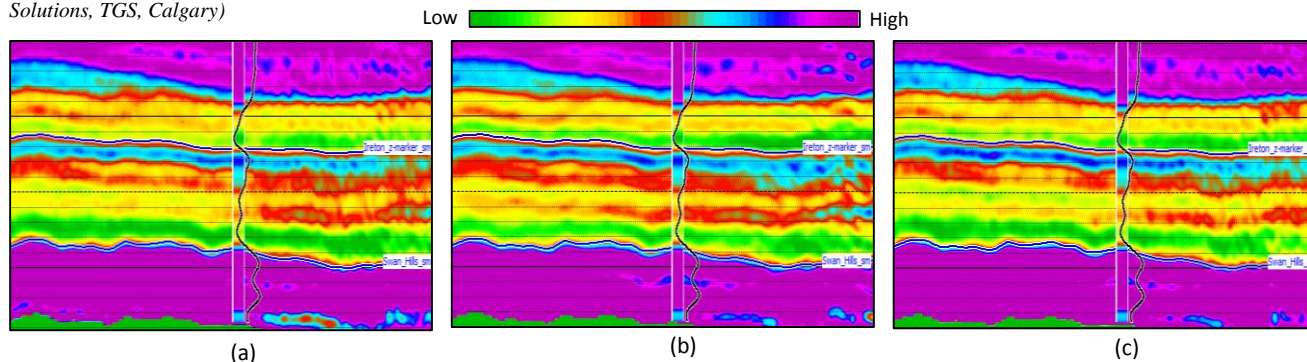


Figure 6: Segment of a section from the impedance volume generated by (a) using prestack simultaneous inversion, (b) poststack joint inversion, and (c) prestack joint inversion. Impedance curve for well W-3 filtered to the seismic bandwidth is shown overlaid on each of the sections. (Data courtesy: Arcis Seismic Solutions, TGS, Calgary)

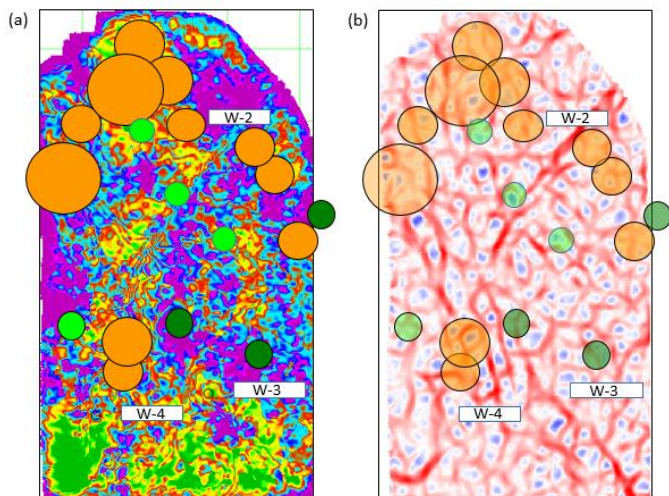


Figure 7: (a) Horizon slice from the brittleness coefficient averaged within the Duvernay zone with the induced seismicity events recorded by the seismic networks overlaid. Events with moment magnitude less than 2 are in light green colour, dark green represents events with magnitude between 2 and 3, pale-yellow represents magnitude greater than 3. Notice that the circles fall in those areas on the brittleness coefficient display that are in purple colour, or pockets which are highly brittle. In the absence of image logs in the area and the accuracy of the exact depth of seismicity events, a conclusive inference about their correlation may be elusive. (Data courtesy: Arcis Seismic Solutions, TGS, Calgary)

## EDITED REFERENCES

Note: This reference list is a copyedited version of the reference list submitted by the author. Reference lists for the 2016 SEG Technical Program Expanded Abstracts have been copyedited so that references provided with the online metadata for each paper will achieve a high degree of linking to cited sources that appear on the Web.

## REFERENCES

- Alberta Energy Regulator (AER), 2016, Seismicity in Alberta, <https://www.aer.ca/about-aer/spotlight-on/seismicity-in-alberta>, accessed 19 February 2016.
- Atkinson, G. M., D. W. Eaton, H. Ghofrani, D. Walker, B. Cheadle, R. Schultz, R. Shcherbakov, K. Tiampo, J. Gu, R. M. Harrington, Y. Liu, M.V. der Baan, and H. Kao, 2016, Hydraulic fracturing and seismicity in the Western Canada Sedimentary Basin: *Sedimentological Research Letters*, **87**, no. 3, 1–17.
- Chopra, S., 2015, The buzz about quantitative seismic interpretation: Presented at the Arcis Symposium in September 2015.
- Chopra, S., and R. K. Sharma, 2015a, Impedance inversion's value in interpretation: *AAPG Explorer*, **36**, 42–53.
- Chopra, S., and R. K. Sharma, 2015b, Impedance inversion: big aid in interpretation: *AAPG Explorer*, **36**, 34–35.
- Cui, L., 2015, Characterizing seismicity in Alberta for induced-seismicity application, <http://ir.lib.uwo.ca/etd/3347/>, accessed 23 March 2016.
- Greiser, B., and J. Bray, 2007, Identification of production potential in unconventional reservoir: Presented at the 2007 SPE Production and Operations Symposium held in Oklahoma City, Oklahoma, U.S.A., 31 March–3 April.
- Ray, A. K., and S. Chopra, 2015, More robust methods of low-frequency model building for seismic impedance inversion: 85th Annual International Meeting, SEG, Expanded Abstracts, 3398–3402, <http://dx.doi.org/10.1190/segam2015-5851713.1>.
- Ray, A. K., and S. Chopra, 2016, Building more robust low-frequency models for seismic impedance inversion: *First Break*, **34**, 29–34.
- Sharma, R. K., and S. Chopra, 2015, Determination of lithology and brittleness of rocks with a new attribute: *The Leading Edge*, **34**, 554–564, <http://dx.doi.org/10.1190/tle34050554.1>.
- USGS, 2016, Earthquake hazards program, [http://earthquake.usgs.gov/earthquakes/states/top\\_states.php](http://earthquake.usgs.gov/earthquakes/states/top_states.php) accessed 23 March 2016.